Chemical Papers (2023) 77:2697–2705
https://doi.org/10.1007/s11696-022-02659-2

ORIGINAL PAPER

An investigation and analysis of structural and electrochemical properties of highly ionic conductive $La_{2-x}Sr_xSn_2O_{7-\delta}$ electrolyte for SOFC applications

Fatima Melit[1] · Nedjemeddine Bounar[1] · Shabana P. S. Shaikh[2] · Manish Deshpande[3] · Marlu Cesar Steil[4]

Received: 8 June 2022 / Accepted: 30 December 2022 / Published online: 17 January 2023

Abstract

This study primarily focused on the investigation, synthesis and analysis of lanthanum and tin pyrochlores electrolytes for solid oxide fuel cell (SOFC) applications. Ceramic samples with diverse compositions of $La_{2-x}Sr_xSn_2O_{7-\delta}$ ($x=0.05$, 0.1, 0.15, 0.2, 0.25, and 0.3) were synthesized by using solid-state reaction (SSR) methods. The prepared $La_{2-x}Sr_xSn_2O_{7-\delta}$ samples were characterized by using X-ray diffraction, scanning electron microscopy and electrochemical impedance spectroscopy measurements. The results were further interpreted regarding the formation of high oxygen vacancy and structural disorder in the $La_{2-x}Sr_xSn_2O_{7-\delta}$ matrix. The doping of lanthanum (La^{3+}) by strontium (Sr^{2+}) had a beneficial and remarkable effect on the structural and electrical properties: the increase in dopant (Sr) concentration decreased the lattice parameters of the crystalline phase and enhanced the creation of oxygen vacancies, which consequently increased the ionic conductivity and decreased the activation energy. Thus, it could be understood that the studied new $La_{2-x}Sr_xSn_2O_{7-\delta}$ electrolyte would be one of the potential candidates for intermediate temperature SOFC applications.

Keywords Electrolyte · Pyrochlore · Impedance spectroscopy · Ionic conductivity · SOFC

Introduction

Pyrochlores oxides are ceramics with the general formula of $A_2B_2O_7$ (Srivastava 2009; Matović et al. 2019), where A and B represent metals. Pyrochlores are often written as $A_2B_2O_6O'$ in order to distinguish the oxygen atoms (anions) in the two different positions: 48f and 8b (Chartier et al. 2003; Gill et al. 2011; Mustafa et al. 2018). Pyrochlores are classified as ternary oxides, with a space group $Fd\bar{3}m$ and a multiplicity $Z=8$; the A and B sites are generally occupied by metal cations, which can be divalent and pentavalent or trivalent and tetravalent, respectively (Subramanian et al. 1983; Yang et al. 2015). Pyrochlore structure $A_2B_2O_6O'$ is considered to be derived from the fluorite structure through doubling the unit cell by removing one of the eight anions and placing cations and anions in four fully occupied and non-equivalent sites (Moriga et al. 1989; Mori et al. 2003).

The excellent structural flexibility of pyrochlores reflects many special properties such as ionic conductivity (Yamamura et al. 2003; Díaz-Guillén et al. 2008), magnetic properties (Ewing et al. 2004; Risovany et al. 2006; Gardner et al. 2010), and thermal characteristics (Cao et al. 2004; Pan et al. 2012). These properties enable them to be a potential candidate for use in several fields such as solid oxide fuel cells (SOFC) (Fergus 2006; Hui et al. 2007), for high-temperature catalysis applications (TONG et al. 2013), in magnetic devices applications (Zhang et al. 2017) and for radiation dampers (Zhang et al. 2009).

Recently, many researchers have studied doped $La_2Sn_2O_7$ pyrochlore for different applications. Abdul Quader et al. have shown that Nd doping causes an improvement in the tunability of the energy storage and switching capabilities of these materials (Quader et al. 2020). Substitution of La

✉ Fatima Melit
fatima.melit@univ-jijel.dz

1 LIME Laboratory, University of Jijel, BP 98, 18000 Ouled Aissa, Algeria

2 Chemical Engineering Process Development Division, CSIR-National Chemical Laboratory, Pune 411008, India

3 Department of Physics, Netaji Subhash Chandra Bose College, Nanded, India

4 Laboratory of Electrochemistry and Physic- Chemistry of Materials and Interfaces, UMR 5279, CNRS-Grenoble INP-UJF, BP75, 38402 Saint Martin d´Hères, France

with Dy3+, Ce3+, Tb3+ Eu3+ showed an improvement in the luminescent properties (Wang et al. 2007; Fu et al. 2009; Yang et al. 2011). It was also noticed an improvement in the conductivity of the structures when the A site was substituted by smaller cations, due to their lower cationic radius ratio, which induces cationic disorder in the structure. This caused ionic conduction in the material (Sergienko et al. 2004).

Among the different types of pyrochlores, the lanthanum and tin-based pyrochlores with the chemical formula of $La_2Sn_2O_7$ (LSO) exhibit highly crystalline structure (Kaliyaperumal et al. 2020). In this class of LSO pyrochlores, the La^{3+} cations are surrounded by eight oxygen atoms that form deformed cubes, whereas the Sn^{4+} cations are located in the center of the trigonal anti-prisms with the six oxygen atoms equidistant from each cation (Subramanian et al. 1983).

This special crystal structure of LSO provides interesting properties such as a large coefficient of thermal expansion, a relatively high melting point (> 2000 °C), excellent conductivity, good luminescence properties and high thermal stability (Xia et al. 2010).

Several types of pyrochlores are widely studied for their electrical properties and application in SOFCs (Yamamura et al. 2003; Díaz-Guillén et al. 2008; Gill et al. 2012; Walker et al. 2013; Valdés-Ibarra et al. 2019). Researchers like C. Kaliyaperumal et al. (2020) had studied the electrical properties of pure$La_2Sn_2O_7$ pyrochlore. The activation energy for conduction from the previous study was reported as 0.87 eV, which is close to the migration of oxygen ions in materials ceramics.

In the present study, efforts were taken to enrich the literature by studying the electrical properties of the doped $La_2Sn_2O_7$ pyrophore. The present work describes the new investigation, synthesis and characterization of LSSO pyrochlore structure based on lanthanum (La_2O_3) and tin (SnO_2) oxides having a general formula $La_2Sn_2O_7$, where 'Sr' substitutes La as an electrolyte material for SOFC.

The main aim was to investigate the structural evolution of the new $La_2Sn_2O_7$ pyrophore as a function of the dopant (Sr) concentration for the creation of oxygen vacancies to promote cation migration through the structural matrix and improve ionic conductivity. Accordingly, the morphology and electrochemical properties of the pyrophore as an electrolyte for SOFC were analysed in depth.

Experimental procedure

Method of synthesis

The samples $La_{2-x}Sr_xSn_2O_{7-\delta}$ ($x = 0.05$–0.3) were synthesized by SSR technique (Zhao et al. 2017). The SnO_2 (Sigma-Aldrich 99.9%), La_2O_3 (Sigma-Aldrich 99.9%) and $SrCO_3$ (Sigma-Aldrich 99.9%) powders were weighed according to the stoichiometric ratio. The powders were crushed in an agate mortar and then compressed into cylindrical discs (13 mm diameter and 0.5 mm thickness) using a uniaxial press, with a pressure of 6–7 tons. After pelletizing, the ground samples were heated at 500 °C for 12 h to decompose the strontium carbonate. Subsequently, the samples were sintered in two cycles: initially at 1000 °C for 48 h and then at 1200 °C for 72 h, to provide the energy required for inter-diffusion of the oxides and crystallization of the pyrochlore phase. To densify the samples, another heat treatment at 1500 °C was carried out for 2 h with a heating rate of 12.5 °C/min. After sintering, $_x$ all $La_{2-x}Sr_xSn_2O_{7-\delta}$ samples were characterised structurally, morphologically and electrically.

Characterizations

The prepared samples were subjected to structural characterization by X-ray powder diffraction XRD. The X-ray diffractograms were recorded in $\theta/2\theta$ Bragg Brentano configuration using a (PANalytical X'Pert PRO MPD) diffractometer with a fixed horizontal sample holder.

The X-ray diffractograms were recorded in the angular domain $2\theta = 10$–$120°$ with a step of 0.017°. The unit cell parameter was determined by the complete decomposition of the pattern according to the Lebail method by using the Rietica software (Howard et al. 1997).

The surface morphologies of the pellets were observed with SEM (PHILIPS XL 30) apparatus. Before SEM, the sintered pellets were coated with a thin layer of gold to avoid the charging effect during measurement.

The electrochemical impedance spectroscopy (EIS) measurements were taken on sintered pellets of 8 mm diameter and 5 mm thickness; the sample pellets were prepared by uniaxial pressing of the fine powder obtained by milling followed by heat treatment at 1500 °C for 2 h. Colloidal platinum (Pt) paint was coated on both sides of the pellets to serve as blocking electrodes and to make conducting points for the impedance measurement.

The impedance data were recorded over 100 Hz–7 MHz frequency range as a function of temperature by using a Frequency Response Analyzer (Hewlett Packard 4192A). The impedance spectra were recorded under dry air at 50 °C intervals in the temperature range of 550–900 °C with a stabilization time of 60 min for each temperature measuring point.

The heating rate between the bearings was kept at 1 K min^{-1}. The rate during the heating cycle was maintained at 50 °C min^{-1} from 550 to 900 °C and air partial pressure of 1 atm, while in the cooling cycle, the temperature of the sample was decreased by 20 °C min^{-1}. The EIS spectra were

analyzed using Z-View software (Scribner Associates INC, version 3.1c).

The synthesis samples were denoted with codes such that initial three letters, i.e., LSS, indicated the chemical name ($La_{2-x}Sr_xSn_2O_{7-\delta}$), followed by a number representing the doping amount of Sr.

Results and discussion

Relative density

The experimental density (ρ) of the studied sample was determined by considering the geometric dimension of the pellet using a Vernier caliper, as shown in Eq. 1 (Appendices). The relative density was calculated as the ratio of experimental and theoretical density values.

From the reported study it is understood that an acceptable relative density of the electrolyte for SOFC was reported to be 94% (Mori et al. 2003; Gill et al. 2011). In general, the relative density obtained for the materials in this current study is approximately 60%. To increase the density further, we carried out very fine grinding and sintering at high temperatures. With further homogeneous grinding and heat treatment, the density of the samples is found to be around 90% as shown in Table 1.

X-ray diffraction analysis (XRD)

The XRD patterns of the pyrochlore compounds are shown in Fig. 1a. Evidently, it was tractable that all the samples showed typical diffraction patterns of $La_2Sn_2O_7$ which is in well agreement with the JCPDS file No. 13-0082 data with pyrochlore structure conforming to the $Fd\bar{3}m$ space group. In the $La_{2-x}Sr_xSn_2O_{7-\delta}$ phases for the substitution rates $x \leq 0.15$, the substitution of the La^{3+} cation by Sr^{2+} led to an almost linear decrease in the mesh parameters and the probability of Sr^{2+} occupation at site A.

Similar results were also reported for high ionic radius dopants for different pyrochlore systems (Díaz-Guillén et al. 2009; Orlovskaya et al. 2011; Krasnov et al. 2018; Valdés-Ibarra et al. 2019). The concentration of the higher rate of substitution ($x = 0.2$, 0.25, and 0.3) led to the formation of the majority phase $La_2Sn_2O_7$ with minor traces of the $SrSnO_3$ phase.

From the obtained XRD pattern, it is apparent that the substitution of cation A in the pyrochlore structure by a cation B having a larger cationic radius leads to an expansion of the unit cell. On the other hand, the substitution by a cation of a lower valence state causes an electronic imbalance in the pyrochlore lattice, which can be compensated either by the generation of a lack of oxygen or by a change of the cationic site B to a higher oxidation state, which is closely inconsistent with the data reported elsewhere (Gill et al. 2011). The higher oxidation state has smaller ionic radii, which leads to a contraction of the lattice parameter as observed in many doped perovskites (Ciambelli et al. 2000; Ciambelli et al. 2001; Abdel-Khalek and Mohamed 2013).

The evolution of cell parameter 'a' of samples $La_{2-x}Sr_xSn_2O_{7-\delta}$ is shown in Fig. 1b as a function of x, the substitution of La^{3+}($r = 1.16$ Å) by a larger cation Sr^{2+} ($r = 1.26$ Å) possessing a lower valence state which leads to a competition between the size effect and the charge effect that has been translated by a linear reduction in the lattice parameters until stabilization for $x > 0.2$; this is due to the solubility limit of strontium in the structure. The observed results are in good agreement with several doped reported pyrochlores studies (Gill et al. 2011; Gill et al. 2012; Krasnov et al. 2018; Matović et al. 2019; Kaliyaperumal et al. 2020).

Scanning electron microscopy (SEM)

The SEM analyses shown in Fig. 2 were performed in order to study the microstructure of porosity and density as a function of the dopant (Sr) concentration. The porosity is directly associated with the ionic conduction (Froboese et al. 2019). For the studied sample, it is observed that the grain size significantly increases with the increase in doping concentration; on the other hand, the porosity decreases with

Table 1 Comparative study of relative density, unit cell parameter, bulk conductivity and activation energy of Sr-doped $La_{2-x}Sr_xSn_2O_7$ ($x = 0.05$ to 0.3)

Sample label	Relative density (%)	Unit cell parameter (Å)	Bulk conductivity σ (S cm^{-1})			E_{aB} (eV) bulk	E_{agb} (eV) GB
			800 °C	850 °C	900 °C		
LSS0.05	86.86	10.69919	1.01×10^{-5}	1.66×10^{-5}	3.35×10^{-5}	1.56	2.06
LSS0.1	95.53	10.69630	2.36×10^{-5}	4.74×10^{-5}	9.11×10^{-5}	1.60	1.99
LSS0.15	98.41	10.67768	4.72×10^{-5}	1.95×10^{-4}	6.65×10^{-4}	1.70	2.26
LSS0.2	98.5	10.67008	1.63×10^{-4}	4.01×10^{-4}	7.58×10^{-4}	1.37	1.81
LSS0.25	97.55	10.66904	2.19×10^{-4}	6.84×10^{-4}	1.63×10^{-3}	1.54	1.69
LSS0.3	92.66	10.66902	2.07×10^{-4}	5.51×10^{-4}	2.13×10^{-3}	1.45	1.67

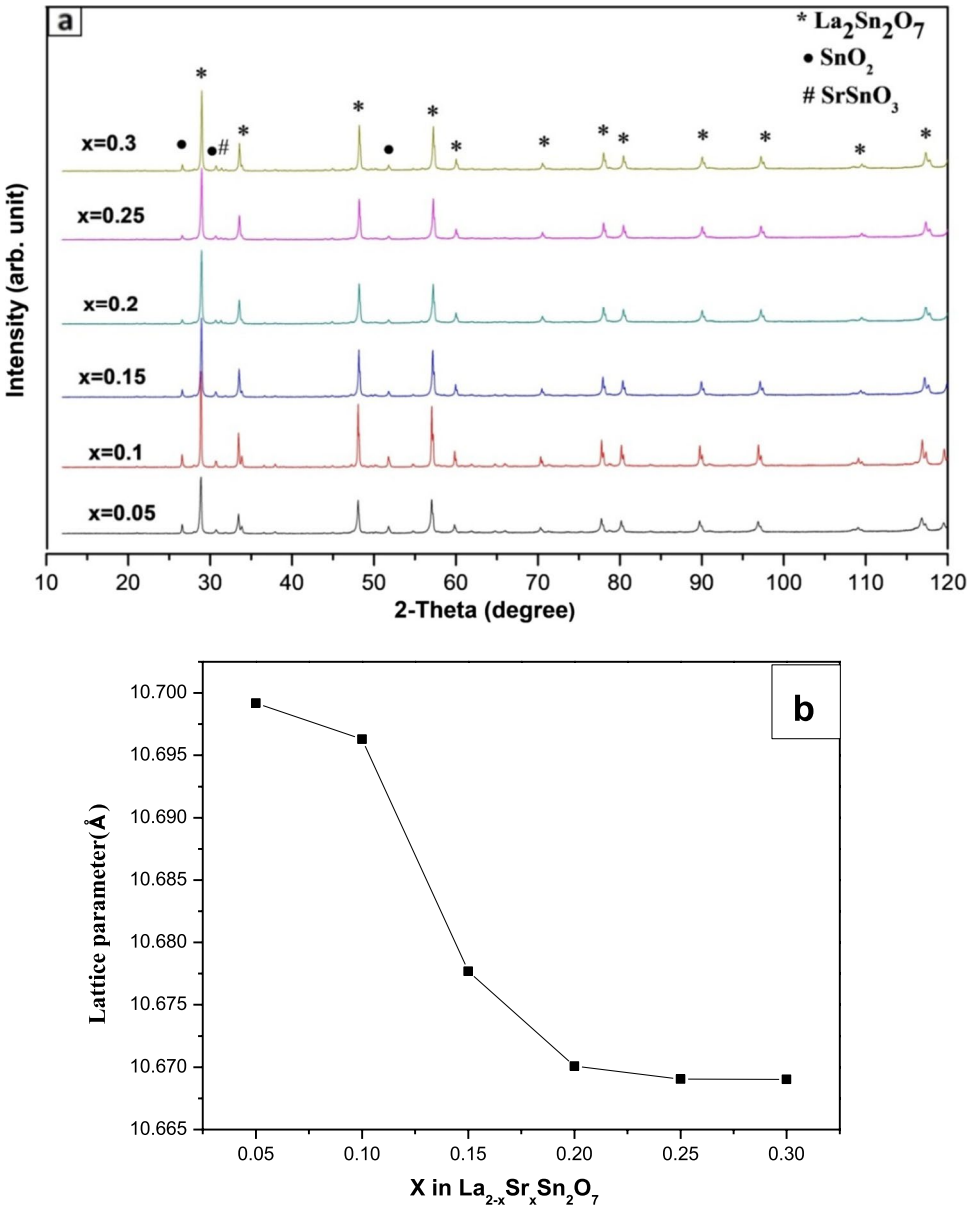

Fig. 1 **a** X-ray diffraction patterns of different $La_{2-x}Sr_xSn_2O_{7-\delta}$ samples prepared with varying doping composition for $x = 0.05–0.3$ **b** The lattice parameters as a function of Sr concentration

the increase in doping concentration in Sr which is further even increasing the density. According to the SEM microphotographs, it is concluded that the prepared electrolyte $La_{2-x}Sr_xSn_2O_7$ has high density which substitutes the higher ionic conductivity explained in detail in further section.

Electrochemical impedance spectroscopy (EIS)

The electrochemical complex impedance spectra of $La_{2-x}Sr_xSn_2O_7$ samples for $x = 0.05–0.3$ recorded and analyzed as an electrolyte for SOFC applications in the dry air environment. All the impedance spectra obtained for the $La_{2-x}Sr_xSn_2O_7$ ceramic ($x = 0.05–0.3$) have the same appearance, and they are also similar to those of most solid electrolyte systems. Figure 3 shows an example of typical impedance spectra obtained at different temperatures for LSSO for sample $x = 0.3$.

The impedance curve at low temperatures (i.e., 550–700 °C) shows the presence of two incomplete and partially resolved semicircles. This may be due to the different relaxation times for the transfer of oxygen ions through bulk, grain boundaries and electrolyte–electrode interfaces (Shaikh and Rode 2020). Furthermore, the depressed arc shows the distribution of current and electroactive species due to the non-ideal capacitive properties of $La_{2-x}Sr_xSn_2O_{7-\delta}$. In this case, the equivalent circuit (R-CPE)b-(R-CPE)gb is used to match data impedances to calculate bulk (Rb) and grain boundary (Rgb) resistances. At higher operating temperatures in the range 750–900 °C, the response of the impedance arc shifts to the higher-frequency

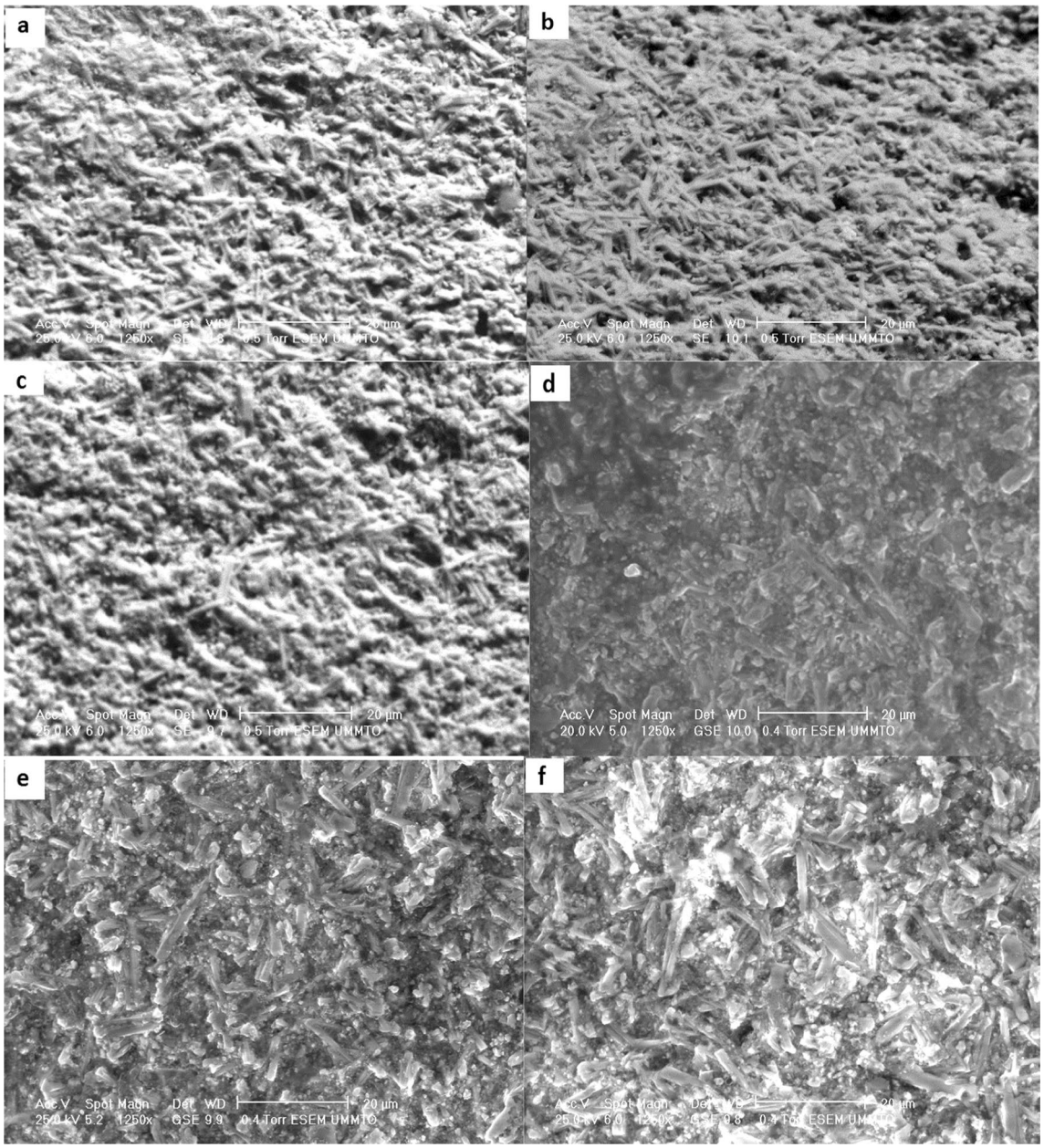

Fig. 2 SEM images of $La_{2-x}Sr_xSn_2O_{7-\delta}$ **a** $x=0.05$ **b** $x=0.1$ **c** $x=0.15$ **d** $x=0.2$ **e** $x=0.25$ and **f** $x=0.3$

region, forming two incomplete semicircles, corresponding to the grain boundary response and the electrolyte–electrode interfaces (Shaikh and Rode 2020).

This observation is due to the decrease in relaxation time and increase in relaxation frequency of the various electrolyte compartments studied with increasing temperature (Xia et al. 2010); an equivalent circuit R_b $(R\text{-}CPE)_{gb}$-$(R\text{-}CPE)$ is used to adapt the data. The resistance of the samples decreases with increasing temperature, which is the manifestation of ionic conductors at high temperature.

Electrical conductivity (σ_{ac}) was calculated based on the observed resistance values from the complex impedance plots fitting using equation Eq. 2 (Appendices) (Gill et al. 2011). The obtained results are depicted in Table 1. Figure 4 reveals the variation of the bulk conductivity as a function of the dopant (Sr) concentration in $La_{2-x}Sr_xSn_2O_7$ at constant temperature; it is clear that the latter increases with the increase in the rate of substitution of lanthanum by strontium, and the increase is due to the creation of oxygen vacancies in the matrix which facilitates the mobility of oxygen.

Sr doping also has a strong effect on the electrical properties of $La_2Sn_2O_7$; with the increase in the dopant (Sr) concentration, there was a significant increase in this conductivity due to the creation of oxygen vacancies. In ionic

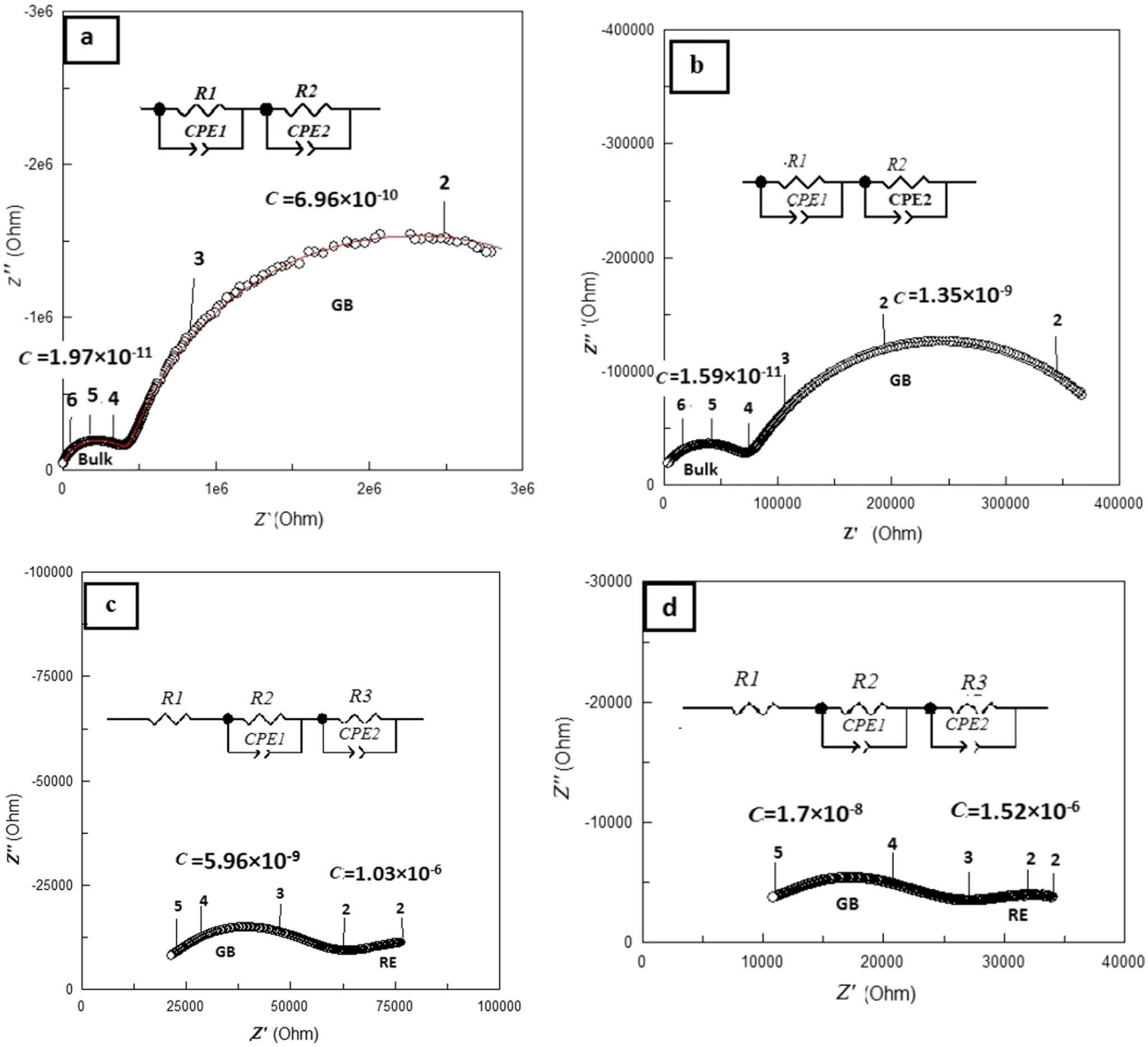

Fig. 3 Impedance spectra of LSS0.3 at **a** 550 °C. **b** 650 °C. **c** 750 °C and **d** 850 °C

conductors, charge transport is given by the hopping of charged O^{2-} ions to neighboring vacant positions in the crystal structure, in a process whose probability of success is thermally activated (Moreno et al. 2005; Traqueia et al. 2006).

In addition, ionic conductors opposed an energy barrier to jump out of their position and contribute to charge transport. This activation energy for the conduction process is denoted by E_a (Valdés-Ibarra et al. 2019).

The activation energy of bulk and grain boundary can be calculated from the Arrhenius plot as shown in Fig. 5. From the obtained plots, it is depicted that the results are in good agreement with the reported date (Valdés-Ibarra et al. 2019), which shows the thermally activated processed generally generates straight lines whose slope is proportional to the activation energy associated with long-range conduction (E_a). The calculated ionic conductivity and activation energy of $La_{2-x}Sr_xSn_2O_7$. The dopant composition that varies from x = 0.05–0.3 is shown in Table 1.

The Sr doping increases the conductivity from 3.35×10^{-5} S cm^{-1} for $x = 0.05$ to the highest value of 2.133×10^{-3} S cm^{-1}, $x = 0.3$ for a fixed temperature of 900 °C. These results are observed significantly better than those found for undoped $La_2Sn_2O_7$ (2.24×10^{-7} S cm^{-1} at 700 °C) (Abdel-Khalek and Mohamed 2013). The conductivity values are also similar to the various results reported in the literature

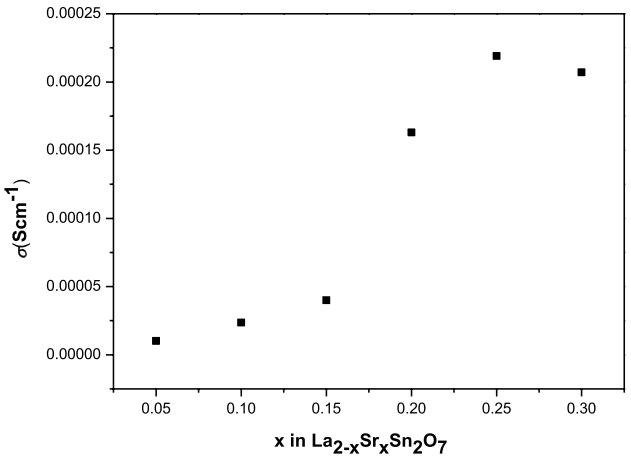

Fig. 4 Variation of the bulk conductivity as a function of the Sr doping rate i in $La_{2-x}Sr_xSn_2O_7$ at 800 °C

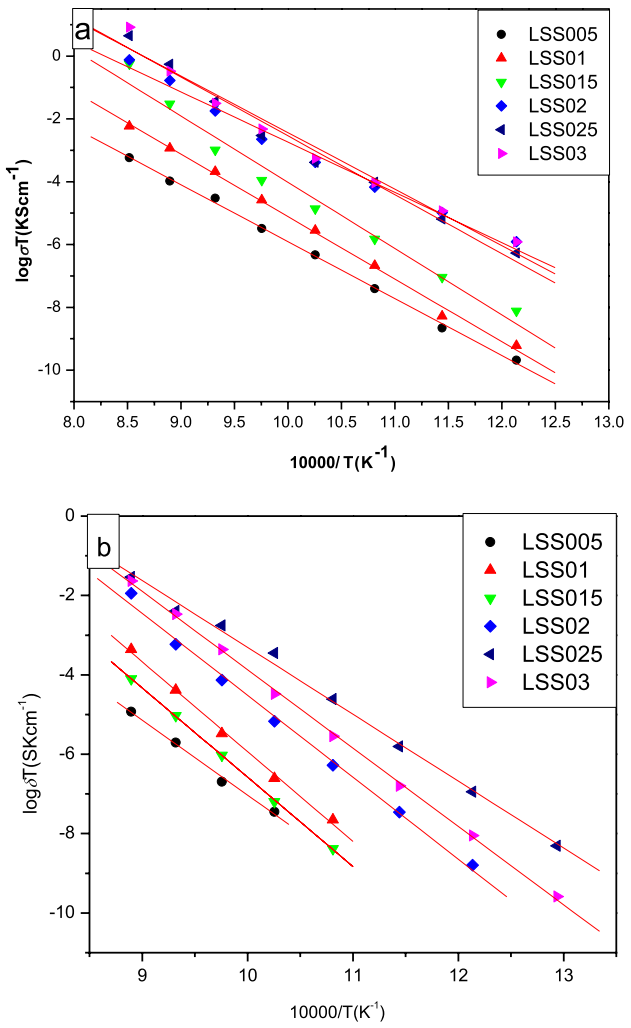

Fig. 5 Arrhenius plots of conductivity for different $La_{2-x}Sr_xSn_2O_{7-\delta}$ samples prepared with varying doping amount for $x = 0.05$–0.3, **a** bulk, **b** grain boundary

for different pyrochlores: 10^{-4} S cm^{-1} at 750 °C for Ca-doped $Bi_2Ti_2O_7$ (Barbero et al. 2006), 10^{-3} at 900 °C for Sr-doped $Y_2Ti_2O_7$ (Barbero et al. 2006), 4.02×10^{-7} S cm^{-1} at S cm^{-1}at 700 °C for Ca-doped Ca-doped $Gd_2Ti_2O_7$. In the present study, the activation energy is found to be in the range of 1.37–1.7 eV as shown in Table 1, which is in good agreement with the previous work (Yang et al. 2015; Jin et al. 2019; Valdés-Ibarra et al. 2019).

Conclusions

The substitution of La^{3+} by Sr^{2+} in $La_2Sn_2O_7$ demonstrated a remarkable effect on the studied electrolyte material concerning structural and electrical properties. The increase in the doping rate induces a modification of the microstructure.

This modification reflected shows that there is a decrease in the lattice parameters of the samples and an improvement in their ionic conductivity. The increase in the lattice is due to the creation of oxygen vacancies due to the dopant species substitutions in the host matrix of $La_{2-x}Sr_xSn_2O_7$, which facilitates the process of ion migration. 'E_a' values decrease as the percentage of strontium replacement increases, which demonstrating that the barrier for an oxygen ion to migrate is lower.

The highest ionic conductivity for the studied $La_{2-x}Sr_xSn_2O_7$ for $x = 0.3$ was found to be 2.133×10^{-3} S cm^{-1} at 900 °C with an activation energy of 1.45 eV. Thus, from the detailed study of structural, morphological and electrochemical characterization and analysis of $La_{2-x}Sr_xSn_2O_7$ ($x = 0.05$–0.3), although the conductivity values are lower for other electrolytes GDC (7.3 10^{-2} S cm^{-1}), YDC (2.0 10^{-2} S cm^{-1}), YZS (2.5 10^{-2}cm S^{-1})(Fergus 2006), it is concluded that the synthesized $La_{2-x}Sr_xSn_2O_7$ with $x = 0.3$ may be one of the emerging potential candidates as a highly densed electrolyte material for SOFC applications.

Appendix

Equation 1:

$$\rho = \frac{4 \times m}{\pi \times d^2 \times e} \tag{1}$$

where 'e' is the pellet thickness, 'm' is the mass of the pellet, and 'd' is the diameter of the pellet.

Equation 2:

$$\sigma_{ac} = \frac{l}{RA} \tag{2}$$

where '*l*' is the thickness of the pellet, '*A*' is the cross section of the pellet, and '*R*' is the resistance of bulk.

Acknowledgements Authors are thankful to the members of the M2E platform at the Laboratory of Electrochemistry and Physical chemistry of Materials and Interfaces in Grenoble, France, for facilitating X-ray analysis and complex impedance spectroscopy as well as for providing their laboratory for experimental study. Also, special thanks to LIME Laboratory, University of Jijel, BP 98 Ouled Aissa, 18000, Algeria.

Declarations

Conflict of interest This is to declare that there is no competing interest or conflict of interest among all authors. All authors are mutually agreed to submit this manuscript for publication. Also, there is no conflict of interest of any of the organization in publishing the present work.

References

Abdel-Khalek E, Mohamed HM (2013) Synthesis, structural and magnetic properties of $La_{1-x}Ca_xFeO_3$ prepared by the co-precipitation method. Hyperfine Interact 222:57–67

Barbero BP, Gamboa JA, Cadus LE (2006) Synthesis and characterisation of $La_{1-x}Ca_xFeO_3$ perovskite-type oxide catalysts for total oxidation of volatile organic compounds. Appl Catal B Environ 65:21–30

Cao X, Vassen R, Stover D (2004) Ceramic materials for thermal barrier coatings. J Eur Ceram Soc 24:1–10

Chartier A, Meis C, Crocombette J-P et al (2003) Atomistic modeling of displacement cascades in $La_2Zr_2O_7$ pyrochlore. Phys Rev B 67:174102

Ciambelli P, Cimino S, De Rossi S et al (2000) $AMnO_3$ (A = La, Nd, Sm) and $Sm_{1-x}Sr_xMnO_3$ perovskites as combustion catalysts: structural, redox and catalytic properties. Appl Catal B Environ 24:243–253

Ciambelli P, Cimino S, Lisi L et al (2001) La, Ca and Fe oxide perovskites: preparation, characterization and catalytic properties for methane combustion. Appl Catal B Environ 33:193–203

Díaz-Guillén J, Díaz-Guillén M, Padmasree K et al (2008) High ionic conductivity in the pyrochlore-type $Gd_{2-y}La_yZr_2O_7$ solid solution ($0 \le y \le 1$). Solid State Ionics 179:2160–2164

Díaz-Guillén J, Fuentes A, Díaz-Guillén M et al (2009) The effect of homovalent A-site substitutions on the ionic conductivity of pyrochlore-type $Gd_2Zr_2O_7$. J Power Sour 186:349–352

Ewing RC, Weber WJ, Lian J (2004) Nuclear waste disposal—pyrochlore ($A_2B_2O_7$): nuclear waste form for the immobilization of plutonium and "minor" actinides. J Appl Phys 95:5949–5971

Fergus JW (2006) Electrolytes for solid oxide fuel cells. J Power Sour 162:30–40

Froboese L, Van Der Sichel JF, Loellhoeffel T et al (2019) Effect of microstructure on the ionic conductivity of an all solid-state battery electrode. J Electrochem Soc 166:A318

Fu Z, Yang HK, Moon BK et al (2009) $La_2Sn_2O_7$: Eu^{3+} micronanospheres: hydrothermal synthesis and luminescent properties. Crys Growth Des 9:616–621

Gardner JS, Gingras MJ, Greedan JE (2010) Magnetic pyrochlore oxides. Rev Mod Phys 82:53

Gill JK, Pandey O, Singh K (2011) Ionic conductivity, structural and thermal properties of pure and Sr^{2+} doped $Y_2Ti_2O_7$ pyrochlores for SOFC. Solid State Sci 13:1960–1966

Gill JK, Pandey O, Singh K (2012) Ionic conductivity, structural and thermal properties of Ca^{2+} doped $Y_2Ti_2O_7$ pyrochlores for SOFC. Int J Hydrog Energy 37:3857–3864

Howard C, Hunter B, Swinkels D (1997) Rietica IUCR. Powder Diff 22:21

Hui SR, Roller J, Yick S et al (2007) A brief review of the ionic conductivity enhancement for selected oxide electrolytes. J Power Sour 172:493–502

Jin Y-J, Liu Z-G, Cao G et al (2019) Microstructure and electrical property of $GdSmZr_2O_7$ doped by rare-earth Ce. Ceram Int 45:8707–8712

Kaliyaperumal C, Jayabalan S, Sankarakumar A et al (2020) Structural and electrical characteristics of nanocrystalline $La_2Sn_2O_7$ pyrochlore. Solid State Sci 105:106245

Krasnov A, Shein I, Piir I et al (2018) Bismuth titanate pyrochlores doped by alkaline earth elements: first-principles calculations and experimental study. Solid State Ionics 317:183–189

Matović B, Maletaškić J, Yoshida K et al (2019) Synthesis, characterization and sintering of fluorite and pyrochlore-type compounds: $Pr_2Zr_2O_7$, $Sm_2Zr_2O_7$ and $PrSmZr_2O_7$. Mater Today Proc 16:156–162

Moreno K, Mendoza-Suárez G, Fuentes A et al (2005) Cooperative oxygen ion dynamics in $Gd_2Ti_{2-y}Zr_yO_7$. Phys Rev B 71:132301

Mori M, Tompsett GM, Sammes NM et al (2003) Compatibility of $Gd_xTi_2O_7$ pyrochlores ($1.72 \le x \le 2.0$) as electrolytes in high-temperature solid oxide fuel cells. Solid State Ionics 158:79–90

Moriga T, Yoshiasa A, Kanamaru F et al (1989) Crystal structure analyses of the pyrochlore and fluorite-type $Zr_2Gd_2O_7$ and anti-phase domain structure. Solid State Ionics 31:319–328

Mustafa GM, Atiq S, Abbas SK et al (2018) Tunable structural and electrical impedance properties of pyrochlores based Nd doped lanthanum zirconate nanoparticles for capacitive applications. Ceram Int 44:2170–2177

Orlovskaya N, Chen Y, Miller N et al (2011) Glycine–nitrate synthesis of Sr doped $La_2Zr_2O_7$ pyrochlore powder. Adv Appl Ceram 110:54–57

Pan W, Phillpot SR, Wan C et al (2012) Low thermal conductivity oxides. MRS Bull 37:917–922

Quader A, Mustafa GM, Abbas SK et al (2020) Efficient energy storage and fast switching capabilities in Nd-substituted $La_2Sn_2O_7$ pyrochlores. Chem Eng J 396:125198

Risovany V, Zakharov A, Muraleva E et al (2006) Dysprosium hafnate as absorbing material for control rods. J Nucl Mater 355:163–170

Sergienko I, Keppens V, Mcguire M et al (2004) Metallic ferroelectricity in the pyrochlore $Cd_2Re_2O_7$. Phys Rev Lett 92:065501

Shaikh S, Rode CV (2020) Rational synthesis of 10GDC electrolyte through a microwave irradiation GNP facile route for SOFC applications. RSC Adv 10:3020–3028

Srivastava A (2009) Chemical bonding and crystal field splitting of the Eu^{3+} 7F1 level in the pyrochlores $Ln_2B_2O_7$ (Ln = La^{3+}, Gd^{3+}, Y^{3+}, Lu^{3+}; B = Sn^{4+}, Ti^{4+}). Opt Mater 31:881–885

Subramanian M, Aravamudan G, Rao GS (1983) Oxide pyrochlores—a review. Progress Solid State Chem 15:55–143

Tong Y, Qian X, Zhao W et al (2013) Synthesis and catalytic properties of $TiO_2/Nd_2Zr_2O_7$ nanocomposites. J Chin Ceram Soc 41:34–37

Traqueia L, Marques F, Kharton V (2006) Oxygen ion conduction in oxide materials: selected examples and basic mechanisms. BOLETIN-SOCIEDAD ESPANOLA DE CERAMICA Y VIDRIO 45:115

Valdés-Ibarra M, Díaz-Guillén J, Padmasree K et al (2019) Oxygen ion conducting pyrochlore oxides prepared by an ultrasound-assisted wet chemistry route: Ca-doped $Gd_2Ti_2O_7$ nanocrystals. Int J Hydrogen Energy 44:12515–12524

Walker JD, Hayes JR, Gaultois MW et al (2013) A case for oxygen deficiency in $Gd_2Ti_{2-x}ZrxO_7$ pyrochlore-type oxides. J Alloys Compd 565:44–49

Wang SM, Xiu ZL, Lü MK et al (2007) Combustion synthesis and luminescent properties of Dy^{3+}-doped $La_2Sn_2O_7$ nanocrystals. Mater Sci Eng B 143:90–93

Xia XL, Ouyang JH, Liu ZG (2010) Electrical properties of gadolinium–europium zirconate ceramics. J Am Ceram Soc 93:1074–1080

Yamamura H, Nishino H, Kakinuma K et al (2003) Electrical conductivity anomaly around fluorite–pyrochlore phase boundary. Solid State Ionics 158:359–365

Yang J, Su Y, Li H et al (2011) Hydrothermal synthesis and photoluminescence of Ce^{3+} and Tb^{3+} doped $La_2Sn_2O_7$ nanocrystals. J Alloys Compd 509:8008–8012

Yang F, Wang Y, Zhao X et al (2015) Enhanced ionic conductivity in pyrochlore and fluorite mixed phase yttrium-doped lanthanum zirconate. J Power Sour 273:290–297

Zhang J, Lian J, Fuentes AF et al (2009) Enhanced radiation resistance of nanocrystalline pyrochlore $Gd_2(Ti_{0.65}Zr_{0.35})_2O_7$. Appl Phys Lett 94:243110

Zhang H, Haule K, Vanderbilt D (2017) Metal-insulator transition and topological properties of pyrochlore iridates. Phys Rev Lett 118:026404

Zhao Y, Li N, Xu C et al (2017) Abnormal pressure induced photoluminescence enhancement and phase decomposition in pyrochlore $La_2Sn_2O_7$. Adv Mater 29:1701513